PDE-Based Neuro Adaptive Control for Multi-Agent Deployment With Non-Collocated Observer

Zhijie Liu, *Member, IEEE*, Jianhui Zhang, Huiyang Song, Yan Yang, Zhijia Zhao, *Member, IEEE*, and Keum-Shik Hong, *Fellow, IEEE*

***Abstract*— A neuro adaptive control for deploying a partial differential equation-based multi-agent system in 3D space with a non-collocated observer is proposed in this study. Since the full states of the system are unavailable in practice, an observer-based control is developed to ensure stability of the underlying closed-loop system. In addition, the system uncertainty is addressed by introducing a neural network control. By choosing appropriate system parameters, the desired control objectives can be achieved. The proposed strategy is simple to implement and its implementation condition is easily satisfied. Finally, the effectiveness of the designed method is verified by the simulation results.**

***Note to Practitioners*— In this paper, we introduce a neuro-adaptive control strategy for a multi-agent system based on partial differential equations in 3D space, using a non-collocated observer. This approach is particularly relevant for practitioners dealing with dynamic and uncertain environments in control systems. Neural networks are employed to manage system uncertainties, adapting to changing conditions, which is crucial in environments with variable system parameters. The non-collocated observer allows for state estimation, beneficial in situations where direct measurement is impractical. Ensuring the observer's accuracy is key for effective control. Our strategy focuses on simplicity and ease of implementation, making it accessible for integration into existing systems. The observer-based control ensures the stability of the closed-loop system, a critical factor for consistent performance.**

***Index Terms*— Adaptive control, multi-agent systems, partial differential equations, non-collocated observer.**

Manuscript received 24 April 2024; accepted 18 July 2024. Date of publication 20 August 2024; date of current version 12 March 2025. This article was recommended for publication by Associate Editor A. Pietrabissa and Editor M. P. Fanti upon evaluation of the reviewers' comments. This work was supported in part by the National Key Research and Development Program of China under Grant 2023YFB4706400; in part by the National Natural Science Foundation of China under Grant 62103039, Grant 62273112, Grant 62073030, and Grant U20A20225; in part by the Joint Fund of Ministry of Education for Equipment Pre-Research under Grant 8091B03032303; in part by Guangdong Basic and Applied Basic Research Foundation under Grant 2023B1515120018 and Grant 2023B1515120019; in part by the National Research Foundation of Korea funded by the Ministry of Science and ICT, South Korea, under Grant IRIS-2023-00207954; and in part by Beijing Top Discipline for Artificial Intelligent Science and Engineering, University of Science and Technology Beijing. *(Corresponding author: Zhijia Zhao.)*

Zhijie Liu, Jianhui Zhang, Huiyang Song, and Yan Yang are with the School of Intelligence Science and Technology and the Institute of Artificial Intelligence, University of Science and Technology Beijing, Beijing 100083, China (e-mail: liuzhijie2012@gmail.com; 17854117586@163.com; huiyangkly@gmai.com; yangyan@ustb.edu.cn).

Zhijia Zhao is with the School of Mechanical and Electrical Engineering, Guangzhou University, Guangzhou 510006, China (e-mail: zhaozj@gzhu.edu.cn).

Keum-Shik Hong is with the School of Mechanical Engineering, Pusan National University, Busan 46241, South Korea (e-mail: kshong@pusan.ac.kr).

Digital Object Identifier 10.1109/TASE.2024.3439747

I. Introduction

In RECENT years, multi-agent system (MAS) has been widely used because of its high flexibility. Many researchers have begun to study the formation control of MASs, aiming to better enhance their collaborative capabilities [1], [2], [3], [4], [5], [6]. A MAS can accomplish complex tasks through cooperation between agents. Compared to single individuals, MASs offer advantages such as scalability, fault tolerance, and reliability. The purpose of formation control for a MAS is to construct a suitable control protocol to enable a group of agents to maintain a desired formation and reach a prescribed goal trajectory [7].

For the agents modeled by the single-integrator, a distributed formation control method based on relative position estimation was proposed to improve the formation control performance by using the estimated position information [8]. Reference [9] investigated the distributed formation control problem for a MAS with unknown leader velocity, measuring only the relative position information of neighboring agents in a local reference frame, and using the measured information for the control law design. The time-varying formation control in finite time for a high-order MAS with unknown leader inputs and disturbance was studied in [10], and the formation tracking of follower agents was implemented by combining the sliding mode control method and the super-twisting algorithm. The above studies on MASs only considered the interconnected agents modeled by ordinary differential equations (ODEs). The disadvantage of the traditional ODE methods is that the growth in the number of agents would lead to an increase in the number of ODEs, thus making control of large-scale MASs more difficult. Furthermore, the MASs modeled by ODEs are only the functions of time, ignoring the effect of the spatial distribution of agents, and therefore cannot completely describe the true spatiotemporal characteristics of the system.

To circumvent the above issue, a method for establishing a system model based on partial differential equation (PDE) has been proposed [11], [12], [13], [14], [15]. Reference [16] analyzed the dynamics of MASs and verified the feasibility of

modeling a MAS using PDEs. For large-scale heterogeneous nonlinear MAS, [17] presents a novel framework based on PDEs to facilitate their practically finite-time deployment. A control strategy was designed for a finite-dimensional discrete MAS obtained by proper discretization of the continuum model PDEs, and the required communication topology was imposed [18]. PDE modeling has several advantages. First, PDEs combine traditional function analysis and control theory, which can be used effectively to study MASs that require a communication network to connect individuals in the system. Second, compared with ODEs, PDEs can reduce the model complexity of MAS and diminish the side effects on control effectiveness when the agents have limited communication performance and sensor performance. Although there are currently researchers building dynamic models of MASs based on PDEs, they generally assume that the system state is known. However, in practice, it is difficult to accurately obtain the system state [19]. Therefore, an effective method is needed to solve this issue. A widely adopted approach is to use observers to estimate the unmeasurable states of the agents [20], [21], [22], [23]. In [24], an observer based on measurable output information is proposed to overcome the issue of unavailable agent states. Reference [25] designed an observer based on the backstepping method to observe the system states for use as a dynamic triggering condition. In practice, the number of sensors and actuators of MASs often doesnot match due to sensor limitations, and thus the application of collocated observers for estimating agents' unknown states is limited, which further motivates us to employ non-collocated observers for state estimation of the agents.

Since actual MASs are often nonlinear, the linear MASs model obtained by linearization and other methods can reflect only the local and partial characteristics of the nonlinear system. In addition, the actual MAS cannot be modeled accurately owing to factors such as insufficient measurement accuracy, and an insufficient understanding of the mechanism of the actual MAS and its environment. As a result, the obtained system model inevitably contains various uncertainties. An effective means is to introduce the radial basis function (RBF) neural networks to deal with system uncertainty [26], [27]. Two immeasurable physical parameters of the engine system were estimated by using neural networks to attenuate the negative impact of system uncertainty on the air-fuel ratio [28]. Reference [29] introduced an RBF neural network to model the dynamics of the manipulator secondary environment and to estimate its parameters. A neuro robust control algorithm was then designed to handle the system uncertainty. Note that the input vectors of the neural networks in the above studies were measurable. For the input vectors containing unmeasurable elements, the above-mentioned methods will no longer be applicable. This drives us for further investigation.

This study is dedicated to addressing the deployment of MASs in the presence of system uncertainty, taking into account scenarios where not all system states are measurable. Simultaneously considering the coupling of system uncertainty and observer design poses a significant challenge. The main contributions of this study are as follows.

(1) The PDEs are utilized for modeling the MAS, thereby overcoming the limitations of ODE modeling, especially when dealing with a large number of agents. The study concentrates on MAS deployment in 3D space, providing a broader range of application scenarios when compared to 2D deployment [30].
(2) The majority studies made the assumption that the states of the MAS were fully known [31], [32], which is not reflective of reality. In light of situations where not all system states are measurable, an observer is designed to estimate the states of the MAS.
(3) In contrast to the approach taken in [33], which assumed that the system's uncertainty adheres to the Lipschitz condition, an RBF neural network is employed in this paper to address system uncertainty, avoiding the imposition of constraints on it. Additionally, a single-parameter adaptive neural network is introduced to streamline the computational workload during the uncertainty approximation process.

The rest of this paper is structured as follows: Section II furnishes several useful inequalities. Section III outlines the system model and provides an equivalent description. In Section IV, we delve into observer design and observer-based control without uncertainty. Section V tackles the design of a neuro-adaptive observer-based control, taking into account uncertainty. Section VI presents numerical simulation results. Finally, Section VII offers concluding remarks.

Notations: Let R, R^+ and R^p be the set of real numbers, positive real numbers, and p-dimensional Euclidean space with the norm $\|\cdot\|$, respectively. $(*)_x$ and $(*)_{xx}$ separately represent the partial derivatives $\partial(*)/\partial x$ and $\partial(*)^2/\partial^2 x$.The superscript 'T' is used for the transposition of vectors. $\|\cdot\|_2$ denotes the ℓ_2-norm. $\mathcal{L}_2(a,b)$ is the Hilbert space of the square integrable functions $\phi(\xi), \xi \in [a,b]$ with the norm given as $\|\phi\|_{\mathcal{L}_2} = \sqrt{\int_a^b z^2 d\xi}$.

II. Preliminaries

Lemma 1: (A variant of the Poincaré-Wirtinger inequality in the 1D spatial domain [34]). For $\sigma_1 < \sigma_2$ and any vector function $e \in H^1(\sigma_1, \sigma_2)$ and $e \in R^m$, we obtain the function

$$\int_{\sigma_1}^{\sigma_2} (e^T(x) - e^T(x_d))(e^T(x) - e^T(x_d))dx \leq \frac{4\varphi}{\pi^2} \int_{\sigma_1}^{\sigma_2} e_x^T(x) e_x(x) dx \tag{1}$$

where $\varphi = \max(x_d^2, (\sigma_2 - x_d)^2)$, and x_d is a constant between σ_1 and σ_2.

Lemma 2: (Young's inequality [35]). For any vectors e_1 and $e_2 \in R^m$, $g \in R^+$, the following inequality holds

$$e_1^T e_2 \leq \frac{1}{g} e_1^T e_1 + g e_2^T e_2 \tag{2}$$

Lemma 3: (Cauchy-Schwarz inequality [36]). For any vectors x and y in Euclidean space R^n with the standard inner product, the following inequality holds

$$\left|x^T y\right| \leq \|x\| \|y\| \tag{3}$$

Lemma 4: ([37]) Consider the basis functions of a Gaussian RBF neural network (26) with $\hat{s}$ being the input vector. If $\hat{s} = s - \bar{\psi}$ where $\bar{\psi}$ is a bounded vector, and constant $\varepsilon > 0$, then we have

$$h_j(\hat{s}_i(x,t)) = \exp\left[\frac{-\left(\hat{s}_i(x,t) - \mu_j\right)^T\left(\hat{s}_i(x,t) - \mu_j\right)}{\eta_i^2}\right]$$
$$h(\hat{s}_i(x,t)) = h(s_i(x,t)) + \varepsilon(s_i(x,t))h_t(s_i(x,t))$$

where $h_t(s_i(x,t))$ is a bounded vector function, and μ_j is the central vector value.

III. Problem Formulation

A set of agents moving in 3D space with coordinate axes (x, y, z) are considered, and the dynamics of each agent are given as

$$\dot{z}_i = v_i \tag{4}$$

where $z_i \in R^n$, $i = 1, 2, 3$, respectively represent the components of the agent states on the x, y, and z axes. $v_i \in R^n$ is the component of the control for the agent. The aim is to deploy agents on a given C^2 curve $\gamma : [0, 2\pi] \to R^3$.

Denote the line graph with n vertices as $C = \{D, E\}$, where $D = \{d_1, \ldots, d_n\}$ is the vertex set and $E = \{(d_i, d_{i+1}), i = 1, \ldots, n-1\} \cup \{(d_n, d_1)\}$ is the edge set. We assign n points on the curve, denoted as $\gamma(h), \ldots, \gamma(nh)$, where $h = 2\pi/n$. Then, the following displacement-based protocol is given as

$$\begin{aligned}
\dot{z}_1(t) &= a\frac{z_2(t) - z_1(t)}{h^2} - a\frac{\gamma(2h) - \gamma(h)}{h^2} \\
\dot{z}_i(t) &= a\frac{z_{i-1}(t) + z_{i+1}(t) - 2z_i(t)}{h^2} \\
&\quad - a\frac{\gamma((i-1)h) + \gamma((i+1)h) - 2\gamma(ih)}{h^2} \\
&\quad i = 2, \ldots, n-1 \\
\dot{z}_n(t) &= a\frac{z_{n-1}(t) - z_n(t)}{h^2} - a\frac{\gamma((n-1)h) - \gamma(nh)}{h^2}
\end{aligned} \tag{5}$$

where $a > 0$ is a control gain, and guarantees that all agents converge to the formation

$$F := \left\{(z_1, \ldots, z_n) \mid z_i - z_j = \gamma(ih) - \gamma(jh), i \neq j\right\} \tag{6}$$

When the system contains a substantial number of agents, particularly when n is large, the entire group of agents within the system can be viewed as a continuum. Consequently, the collective dynamics of MASs can be represented by PDEs.

This leads to

$$z_t(\alpha, t) = a(z_{\alpha\alpha}(\alpha, t) - \gamma_{\alpha\alpha}(\alpha)) \tag{7}$$

It is worth noting that the MAS (7) is unable to reach the desired curve γ, instead, it attains only a constant translation. Related theories addressing this issue have been explored in [7]. Consequently, an additional controller is required to guide the agents to the designated spatial location while preserving the formation.

Denoting the error $w(x,t) = z(x,t) - \gamma(x)$ and considering the system uncertainty, we arrive at the following error system:

$$\begin{cases}
w_t(x,t) = aw_{xx}(x,t) + u(x,t) + f(s(x,t)) \\
w(0,t) = w(2\pi,t) \\
w_x(0,t) = w_x(2\pi,t)
\end{cases} \tag{8}$$

where $w(x,t) = [w_1(x,t), w_2(x,t), w_3(x,t)]^T, w_i(x,t) \in R^n$. $x \in [0, 2\pi]$ and $t \geq 0$ respectively represent spatial position and time. $u(x,t) = [u_1(x,t), u_2(x,t), u_3(x,t)]^T$ denotes the control input for the agent, with $u_i(x,t) \in R^n$. $f(s(x,t)) = \left[f_1(s(x,t)), f_2(s(x,t)), f_3(s(x,t))\right]^T$ represents the system uncertainty, with $f_i(s(x,t)) \in R^n$ and $s(x,t) = [w(x,t), w_t(x,t)]^T$. The desired formation is a closed C^2 curve, corresponding to the periodic boundary conditions $w(0,t) = w(2\pi,t)$ and $w_x(0,t) = w_x(2\pi,t)$.

Remark 1: The controller to be designed necessitates complete state information regarding the system (8). Nevertheless, in practical scenarios, attaining such information is typically challenging due to device limitations and cost constraints. Hence, a non-collocated observer is required to estimate the unobtainable states of the system, which serves as the driving force behind our proposal for the following outcomes.

IV. Non-Collocated Observer and Observer-Based Control Design

In situations where complete state information of the system (8) is inaccessible, we introduce the subsequent non-collocated observer to estimate the agents' unknown states. Specifically, only one selected agent is able to access its own location, precisely the agent positioned at $x = \pi$. This approach serves to simultaneously decrease the sensor count. The observer is designed as follows:

$$\begin{cases}
\hat{w}_t(x,t) = a\hat{w}_{xx}(x,t) + u(x,t) + P(w(\pi,t) - \hat{w}(\pi,t)) \\
\hat{w}(0,t) = \hat{w}(2\pi,t) \\
\hat{w}_x(0,t) = \hat{w}_x(2\pi,t)
\end{cases} \tag{9}$$

where $\hat{w}(x,t) = \left[\hat{w}_1(x,t), \hat{w}_2(x,t), \hat{w}_3(x,t)\right]^T$ is the estimated state, with $\hat{w}_i(x,t) \in R^n$. P is the observer gain to be designed.

Remark 2: In contrast to [38] and [39], which utilize complete state information of MASs for controller design, our proposed observer-based protocol solely relies on the output information from a single agent.

To obtain the appropriate value of P that guarantees $\hat{w}(x,t)$ converging to $w(x,t)$, we propose $\tilde{w}(x,t) = w(x,t) - \hat{w}(x,t)$ to denote the estimation error of the observer. Thus, we get

$$\begin{cases}
\tilde{w}_t = a\tilde{w}_{xx}(x,t) + f(s(x,t)) - P\tilde{w}(\pi,t) \\
\tilde{w}(0,t) = \tilde{w}(x,t) \\
\tilde{w}_x(0,t) = \tilde{w}_x(2\pi,t)
\end{cases} \tag{10}$$

An observer-based feedback controller is designed to ensure the stability of the system (8) in the case that $f(s(x,t))$ is zero

$$u(x,t) = -k\hat{w}(x,t) - P\tilde{w}(\pi,t) \tag{11}$$

where k is the control gain to be determined. Using the Lyapunov method, and Lemmas 1 and 2, the observer design problem can be solved by the following theorem.

Theorem 1: Assuming $f(s(x,t))$ is zero, we consider the MAS (8) without system uncertainty. For system parameters $a>0, k>0$, and $P>0$, if the following matrix inequalities are fulfilled by choosing proper values,

$$\Xi_1=\begin{bmatrix}\frac{a}{4} & *\\ \frac{2P-a}{4} & \frac{a}{4}\end{bmatrix}>0$$

and

$$\Xi_2=\begin{bmatrix}k+\frac{a}{4} & *\\ -\frac{a}{4} & \frac{a}{4}\end{bmatrix}>0$$

the exponential stability of the error system (8) and (10) can be demonstrated in the sense of $\|\cdot\|_2$.

Proof: Consider a Lyapunov function for the estimation error system

$$V_1(t)=\frac{1}{2}\int_0^{2\pi}\tilde{w}^T(x,t)\tilde{w}(x,t)dx \tag{12}$$

The time derivative of $V_1(t)$ gives

$$\begin{aligned}&\dot{V}_1(t)\\&=\int_0^{2\pi}\tilde{w}^T(x,t)\tilde{w}_t(x,t)dx\\&=\int_0^{2\pi}\tilde{w}^T(x,t)\big[a\tilde{w}_{xx}(x,t)-P\tilde{w}(\pi,t)\big]dx\\&=a\int_0^{2\pi}\tilde{w}^T(x,t)\tilde{w}_{xx}(x,t)dx-P\int_0^{2\pi}\tilde{w}^T(x,t)\tilde{w}(\pi,t)dx\end{aligned} \tag{13}$$

By integrating by parts and applying Lemma 1, we obtain

$$\begin{aligned}a\int_0^{2\pi}\tilde{w}^T(x,t)\tilde{w}_{xx}(x,t)dx&=-a\int_0^{2\pi}\tilde{w}_x^T(x,t)\tilde{w}_x(x,t)dx\\&\le-\frac{a}{4}\int_0^{2\pi}\big[\tilde{w}^T(x,t)-\tilde{w}^T(\pi,t)\big]\big[\tilde{w}(x,t)-\tilde{w}(\pi,t)\big]dx\end{aligned} \tag{14}$$

where the periodic boundary conditions in (10) are considered.

Substituting (14) into (13), we obtain

$$\begin{aligned}&\dot{V}_1(t)\\&=-a\int_0^{2\pi}\tilde{w}_x^T(x,t)\tilde{w}_x(x,t)dx-P\int_0^{2\pi}\tilde{w}^T(x,t)\tilde{w}(\pi,t)dx\\&\le-\frac{a}{4}\int_0^{2\pi}\big[\tilde{w}^T(x,t)-\tilde{w}^T(\pi,t)\big]\big[\tilde{w}(x,t)-\tilde{w}(\pi,t)\big]dx\\&\quad-P\int_0^{2\pi}\tilde{w}^T(x,t)\tilde{w}(\pi,t)dx\\&\le-\frac{a}{4}\int_0^{2\pi}\tilde{w}^T(x,t)\tilde{w}(x,t)dx-\frac{a}{4}\int_0^{2\pi}\tilde{w}^T(\pi,t)\tilde{w}(\pi,t)dx\\&\quad-(P-\frac{a}{2})\int_0^{2\pi}\tilde{w}^T(x,t)\tilde{w}(\pi,t)dx\end{aligned} \tag{15}$$

Form (15), we have

$$\dot{V}_1\le-\int_0^{2\pi}\xi_1\Xi_1{\xi_1}^T dx \tag{16}$$

where $\xi_1=\big[\tilde{w}^T(x,t)\ \tilde{w}^T(\pi,t)\big]$. If the matrix Ξ_1 is positive definite, we can find a constant $\mu_1>0$ such that the inequality (16) is rewritten as

$$\dot{V}_1(t)\le-\mu_1 V_1(t) \tag{17}$$

Thus, the exponential stability of the estimation error system can be guaranteed with suitable observer gain. Next, we consider the following Lyapunov function:

$$V(t)=V_1(t)+V_2(t) \tag{18}$$

$V_2(t)$ is defined as

$$V_2(t)=\frac{1}{2}\int_0^{2\pi}\hat{w}^T(x,t)\hat{w}(x,t)dx \tag{19}$$

The time derivative of $V_2(t)$ yieds

$$\begin{aligned}\dot{V}_2(t)&=\int_0^{2\pi}\hat{w}^T(x,t)\hat{w}_t(x,t)dx\\&=\int_0^{2\pi}\hat{w}^T(x,t)\big[a\hat{w}_{xx}(x,t)+u(x,t)+P\tilde{w}(\pi,t)\big]dx\end{aligned} \tag{20}$$

Integrating by part and using Lemma 1 give

$$\begin{aligned}&a\int_0^{2\pi}\hat{w}^T(x,t)\hat{w}_{xx}(x,t)dx\\&=-a\int_0^{2\pi}\hat{w}_x^T(x,t)\hat{w}_x(x,t)dx\\&\le-\frac{a}{4}\int_0^{2\pi}\big[\hat{w}^T(x,t)-\hat{w}^T(\pi,t)\big]\big[\hat{w}(x,t)-\hat{w}(\pi,t)\big]dx\end{aligned} \tag{21}$$

Substituting (11) and (21) into (20), we obtain:

$$\begin{aligned}\dot{V}_2(t)\le(-k-\frac{a}{4})&\int_0^{2\pi}\hat{w}^T(x,t)\hat{w}(x,t)dx\\&+\frac{a}{2}\int_0^{2\pi}\hat{w}^T(x,t)\hat{w}(\pi,t)dx\\&-\frac{a}{4}\int_0^{2\pi}\hat{w}^T(\pi,t)\hat{w}(\pi,t)dx\end{aligned} \tag{22}$$

Using (15) and (22), the time derivative of $V(t)$ is given as

$$\begin{aligned}\dot{V}(t)&=\dot{V}_2(t)+\dot{V}_1(t)\\&\le(-\frac{a}{4}-k)\int_0^{2\pi}\hat{w}^T(x,t)\hat{w}(x,t)dx\\&\quad+\frac{a}{2}\int_0^{2\pi}\hat{w}^T(x,t)\hat{w}(\pi,t)dx\\&\quad-\frac{a}{4}\int_0^{2\pi}\hat{w}^T(\pi,t)\hat{w}(\pi,t)dx\\&\quad-\frac{a}{4}\int_0^{2\pi}\tilde{w}^T(x,t)\tilde{w}(x,t)dx\\&\quad-\frac{a}{4}\int_0^{2\pi}\tilde{w}^T(\pi,t)\tilde{w}(\pi,t)dx\\&\quad+(\frac{a}{2}-P)\int_0^{2\pi}\tilde{w}^T(x,t)\tilde{w}(\pi,t)dx\\&\le-\int_0^{2\pi}\xi_2\Xi_2{\xi_2}^T dx-\int_0^{2\pi}\xi_1\Xi_1{\xi_1}^T dx\end{aligned} \tag{23}$$

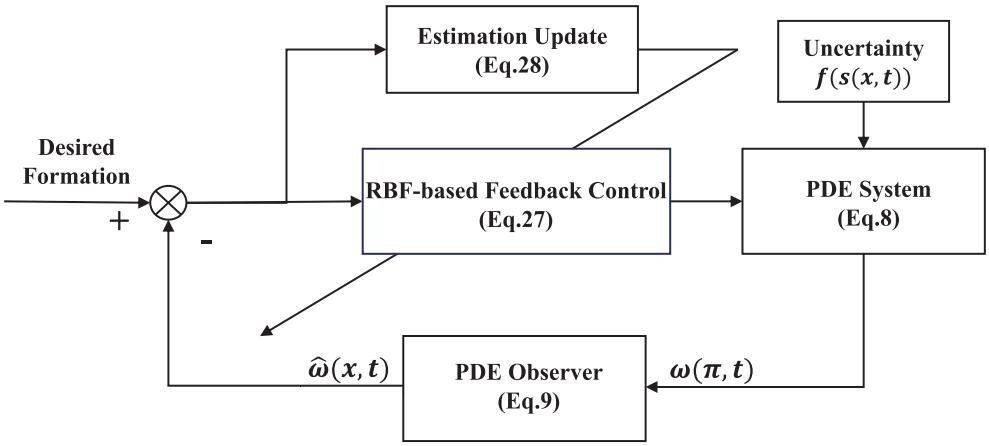

Fig. 1. Diagram for the observer-based neuro adaptive control scheme.

where $\xi_2 = \left[\hat{w}^T(x,t)\ \hat{w}^T(\pi,t)\right]$. Similarly, if the matrices Ξ_1 and Ξ_2 are both positive definite, we can find a constant $\mu_2 > 0$ to obtain the following

$$\dot{V}(t) \le -\mu_2 V(t) \tag{24}$$

From (24), we can deduce that by selecting appropriate controller and observer parameters, we can establish the exponential stability of the closed-loop coupled MAS described by (8) and (10).

Remark 3: In this section, we make the assumption that $f(s(x,t))$ is equal to zero, although achieving this condition in practical scenarios can be challenging. In the subsequent section, we explore the scenario where $f(s(x,t))$ is non-zero.

V. Neuro-Adaptive Control Design

Real-world MASs typically exhibit nonlinear behavior, and due to uncertainties in their dynamic models, accurate modeling becomes challenging. In this section, we focus on a specific type of MAS characterized by uncertainty. To handle the system uncertainty function $\|f(s(x,t))\|$, we introduce an RBF neural network [40], featuring radial basis functions as activation functions, capable of accurately approximating any function with rapid learning convergence speed. We express $\|f(s(x,t))\|$ as a combination of a constant ideal weight W^{*T} and a basis function $h(s(x,t))$. This is achieved as

$$\|f_i(s_i(x,t))\| = W_i^{*T} h_i(s_i(x,t)) + \varepsilon_i(s_i(x,t)) \tag{25}$$

with $s_i(x,t) \in R^m$ being the input of the network and $W_i^{*T} \in R^q$. $\varepsilon_i(s_i(x,t))$ is the approximation error satisfying $|\varepsilon_i(s_i(x,t))| \le \bar{\varepsilon}$, with $\bar{\varepsilon} \in R^+$ being an unknown constant. q denotes the number of neural network nodes and $h_i(s(x,t)) = \left[h_1(s(x,t)), \ldots, h_q(s(x,t))\right]^T \in R^q$ is the RBF neural network architecture employing Gaussian functions in the form of

$$h_j(s_i(x,t)) = \exp\left[\frac{-\left(s_i(x,t)-\mu_j\right)^T\left(s_i(x,t)-\mu_j\right)}{\eta_i^2}\right] \tag{26}$$

where $j = 1, \ldots, q$, $\mu_j \in R^m$ is the center of the receptive field and $\eta_i \in R^+$ is the width of the Gaussian function.

Assumption 1: There is an upper bound on the optimal weight matrices W satisfying $\|W_i^{*T}\| \le W_m^{*T}$.

To alleviate the computational load, we opt to estimate only the weight norm of the neural network. We define $\phi_i(x,t) = \left\|W_i^*\right\|^2$, where $|\phi_i(x,t)| \le \phi_m$ due to assumption 1. $\hat{\phi}(x,t)$ represents the estimation of $\phi(x,t)$, and the error is denoted as $\tilde{\phi}(x,t) = \phi(x,t) - \hat{\phi}(x,t)$. Through the design of an online updating law for the neural network, we ensure that the neural network can meet the accuracy requirements of the function $f(s(x,t))$ and achieve adaptive learning. A flowchart of the MAS is depicted in Fig. 1.

Using the estimated states obtained from the observer, we design the controller as follows:

$$u_i(x,t) = -\frac{g\hat{\phi}_i h^T(\hat{s}_i(x,t))h(\hat{s}_i(x,t))}{2\pi\hat{w}_i(x,t)} - k\hat{w}_i(x,t) - P\tilde{w}_i(\pi,t) \tag{27}$$

where

$$\hat{w}_i(x,t) = \begin{cases} \hat{w}_i(x,t), & \hat{w}_i(x,t) \neq 0 \\ \hat{w}_i(x,t)|_{t=t_0}, & \hat{w}_i(x,t) = 0 \end{cases}$$

The network adaptation law is designed as

$$\dot{\hat{\phi}}_i = \frac{g\beta h^T(\hat{s}_i(x,t))h(\hat{s}_i(x,t))}{2\pi} - \beta\hat{\phi}_i \tag{28}$$

Remark 4: In contrast to the neural network design approach outlined in [41], our method doesnot involve estimating the ideal weights of the RBF neural network; instead, we focus solely on estimating its norm. This design strategy enables us to estimate just one unknown parameter, thereby reducing the computational load on the system.

Theorem 2 offers a method for the feedback control law (27) with observer (9) for the nonlinear MAS described by (8).

Theorem 2: Consider a MAS with uncertainty. For given constants $a > 0$, $P > 0$, and $g > 0$, by choosing appropriate parameters, the following limited matrix inequalities are fulfilled as

$$\Xi_3 = \begin{bmatrix} \frac{a}{4} - \frac{3}{g} & * \\ \frac{2P-a}{4} & \frac{a}{4} \end{bmatrix} > 0$$

$$\Xi_4 = \begin{bmatrix} k + \frac{a}{4} & * \\ -\frac{a}{4} & \frac{a}{4} \end{bmatrix} > 0$$

Then, the MAS is uniformly ultimately bounded in the sense of $\|\cdot\|_2$.

Proof: Consider the Lyapunov function for the MASs (8) and (10)

$$V(t) = V_1(t) + V_2(t) + V_3(t) \tag{29}$$

$V_3(t)$ is defined as

$$V_3(t) = \frac{1}{2\beta}\int_0^{2\pi}\sum_{i=1}^{3}\tilde{\phi}_i^2(x,t)dx \tag{30}$$

where β is the designed constant. The time derivative of $V(t)$ gives

$$\begin{aligned}
&\dot{V}(t)\\
&= \dot{V}_1(t) + \dot{V}_2(t) + \dot{V}_3(t)\\
&= \int_0^{2\pi}\hat{w}^T(x,t)\big[a\hat{w}_{xx}(x,t) + u(x,t) + P\tilde{w}(\pi,t)\big]dx\\
&\quad + \int_0^{2\pi}\tilde{w}^T(x,t)\big[a\tilde{w}_{xx}(x,t) + f(s(x,t)) - P\tilde{w}(\pi,t)\big]dx\\
&\quad - \frac{1}{\beta}\int_0^{2\pi}\sum_{i=1}^{3}\tilde{\phi}_i(x,t)\dot{\hat{\phi}}_i(x,t)dx
\end{aligned} \tag{31}$$

Using the integral by parts, we obtain

$$\begin{aligned}
\dot{V}(t) = &-a\int_0^{2\pi}\hat{w}_x^T(x,t)\hat{w}_x(x,t)dx\\
&- a\int_0^{2\pi}\tilde{w}_x^T(x,t)\tilde{w}_x(x,t)dx\\
&- P\int_0^{2\pi}\tilde{w}^T(x,t)\tilde{w}(\pi,t)dx\\
&- \frac{1}{\beta}\int_0^{2\pi}\sum_{i=1}^{3}\tilde{\phi}_i(x,t)\dot{\hat{\phi}}_i(x,t)dx\\
&+ \int_0^{2\pi}\hat{w}^T(x,t)\big[u(x,t) + P\tilde{w}(\pi,t)\big]dx\\
&+ \int_0^{2\pi}\tilde{w}^T(x,t)f(s(x,t))dx
\end{aligned} \tag{32}$$

By applying Lemmas 1 and 3, and substituting (25) and (27) into (32), we have

$$\begin{aligned}
\dot{V}(t) \le &(-k - \frac{a}{4})\int_0^{2\pi}\hat{w}^T(x,t)\hat{w}(x,t)dx\\
&+ \frac{a}{2}\int_0^{2\pi}\hat{w}^T(x,t)\hat{w}(\pi,t)dx\\
&- \frac{a}{4}\int_0^{2\pi}\hat{w}^T(\pi,t)\hat{w}(\pi,t)dx\\
&- \frac{g}{2\pi}\int_0^{2\pi}\hat{\phi}(x,t)h^T(\hat{s}(x,t))h(\hat{s}(x,t))dx\\
&- \frac{a}{4}\int_0^{2\pi}\tilde{w}^T(x,t)\tilde{w}(x,t)dx\\
&+ (\frac{a}{2} - P)\int_0^{2\pi}\tilde{w}^T(x,t)\tilde{w}(\pi,t)dx\\
&- \frac{a}{4}\int_0^{2\pi}\tilde{w}^T(\pi,t)\tilde{w}(\pi,t)dx\\
&+ \|\tilde{w}(x,t)\|[W^{*T}h(s(x,t)) + \varepsilon(s(x,t))]\\
&- \frac{1}{\beta}\int_0^{2\pi}\sum_{i=1}^{3}\tilde{\phi}_i(x,t)\dot{\hat{\phi}}_i(x,t)dx
\end{aligned} \tag{33}$$

By applying Lemma 4 and using the properties, we have

$$W^{*T}h(s(x,t)) = W^{*T}h(\hat{s}(x,t)) - W^{*T}\varepsilon(s(x,t))h_t(s(x,t)) \tag{34}$$

By using Lemma 2 and 3, we have the following inequalities

$$\begin{aligned}
&\|\tilde{w}(x,t)\|W^{*T}h(\hat{s}(x,t))\\
&\le \frac{1}{g}\|\tilde{w}(x,t)\|^2 + g\|W^{*T}h(\hat{s}(x,t))\|^2\\
&\le \frac{1}{g}\|\tilde{w}(x,t)\|^2 + g\|W^*\|^2\|h(\hat{s}(x,t))\|^2\\
&\le \frac{1}{g}\|\tilde{w}(x,t)\|^2 + g\phi(x,t)h^T(\hat{s}(x,t))h(\hat{s}(x,t))\\
&\quad - \|\tilde{w}(x,t)\|W^{*T}\varepsilon(s(x,t))h_t(s(x,t))
\end{aligned} \tag{35}$$

$$\begin{aligned}
&\le \frac{1}{g}\|\tilde{w}(x,t)\|^2 + g\|W^{*T}\varepsilon(s(x,t))h_t(s(x,t))\|^2\\
&\le \frac{1}{g}\|\tilde{w}(x,t)\|^2 + g\phi_m(x,t)\bar{\varepsilon}^2(s(x,t))h_t^2(s(x,t))
\end{aligned} \tag{36}$$

$$\|\tilde{w}(x,t)\|\|\varepsilon(s(x,t))\| \le \frac{1}{g}\|\tilde{w}(x,t)\|^2 + g\bar{\varepsilon}^2(s(x,t)) \tag{37}$$

Substituting (28), and (35)-(37) into (33) yields

$$\begin{aligned}
\dot{V}(t) \le &(-k - \frac{a}{4})\int_0^{2\pi}\hat{w}^T(x,t)\hat{w}(x,t)dx\\
&+ \frac{a}{2}\int_0^{2\pi}\hat{w}^T(x,t)\hat{w}(\pi,t)dx\\
&- \frac{a}{4}\int_0^{2\pi}\hat{w}^T(\pi,t)\hat{w}(\pi,t)dx\\
&+ (\frac{3}{g} - \frac{a}{4})\int_0^{2\pi}\tilde{w}^T(x,t)\tilde{w}(x,t)dx\\
&+ (\frac{a}{2} - P)\int_0^{2\pi}\tilde{w}^T(x,t)\tilde{w}(\pi,t)dx\\
&- \frac{a}{4}\int_0^{2\pi}\tilde{w}^T(\pi,t)\tilde{w}(\pi,t)dx\\
&+ \int_0^{2\pi}\sum_{i=1}^{3}\tilde{\phi}_i(x,t)\hat{\phi}_i(x,t)dx\\
&+ g\phi_m(x,t)\bar{\varepsilon}^2(s(x,t))h_t^2(s(x,t))\\
&+ g\bar{\varepsilon}^2(s(x,t))
\end{aligned} \tag{38}$$

Consider the following inequality gives

$$\begin{aligned}
&\hat{\phi}_i^2(x,t)\\
&= (\phi_i(x,t) - \tilde{\phi}_i(x,t))^2\\
&= \phi_i^2(x,t) - 2\tilde{\phi}_i(x,t)\phi_i(x,t) + \tilde{\phi}_i^2(x,t)\\
&= \phi_i^2(x,t) - 2\tilde{\phi}_i(x,t)(\tilde{\phi}_i(x,t) + \hat{\phi}_i(x,t)) + \tilde{\phi}_i^2(x,t)\\
&= \phi_i^2(x,t) - 2\tilde{\phi}_i(x,t)\hat{\phi}_i(x,t) - \tilde{\phi}_i^2(x,t) \ge 0
\end{aligned} \tag{39}$$

For (39) we further get

$$\tilde{\phi}_i(x,t)\hat{\phi}_i(x,t) \le \frac{1}{2}(-\tilde{\phi}_i^2(x,t) + \phi_i^2(x,t)) \tag{40}$$

Thus, we have

$$\begin{aligned}
\dot{V}(t) \le\ & (-k - \frac{a}{4}) \int_0^{2\pi} \hat{w}^T(x,t)\hat{w}(x,t)dx \\
& + \frac{a}{2}\int_0^{2\pi} \hat{w}^T(x,t)\hat{w}(\pi,t)dx \\
& - \frac{a}{4}\int_0^{2\pi} \hat{w}^T(\pi,t)\hat{w}(\pi,t)dx \\
& + (\frac{3}{g} - \frac{a}{4}) \int_0^{2\pi} \tilde{w}^T(x,t)\tilde{w}(x,t)dx \\
& + (\frac{a}{2} - P) \int_0^{2\pi} \tilde{w}^T(x,t)\tilde{w}(\pi,t)dx \\
& - \frac{a}{4}\int_0^{2\pi} \tilde{w}^T(\pi,t)\tilde{w}(\pi,t)dx \\
& - \frac{1}{2}\int_0^{2\pi} \sum_{i=1}^{3} \tilde{\phi}_i^2(x,t)dx \\
& + g\phi_m(x,t)\bar{\varepsilon}^2(s(x,t))h_t^2(s(x,t)) \\
& + g\bar{\varepsilon}^2(s(x,t)) + \frac{3}{2}\phi_m^2(x,t) \\
\le & -\int_0^{2\pi} \xi_3 \Xi_3 \xi_3{}^T dx - \int_0^{2\pi} \xi_4 \Xi_4 \xi_4{}^T dx \\
& - \frac{1}{2}\int_0^{2\pi} \sum_{i=1}^{3} \tilde{\phi}_i^2(x,t)dx + g\bar{\varepsilon}^2(s(x,t)) + \frac{3}{2}\phi_m^2(x,t) \\
& + g\phi_m(x,t)\bar{\varepsilon}^2(s(x,t))h_t^2(s(x,t))
\end{aligned} \tag{41}$$

where $\xi_3 = \left[\tilde{w}^T(x,t)\ \tilde{w}^T(\pi,t)\right]$ and $\xi_4 = \left[\hat{w}^T(x,t)\ \hat{w}^T(\pi,t)\right]$.

Considering $\Xi_3 > 0$, $\Xi_4 > 0$, (29), and (41) gives

$$\begin{aligned}
\dot{V}(t) \le & -\lambda V + g\phi_m(x,t)\bar{\varepsilon}^2(s(x,t))h_t^2(s(x,t)) \\
& + g\bar{\varepsilon}^2(s(x,t)) + \frac{3}{2}\phi_m^2(x,t)
\end{aligned} \tag{42}$$

We denote $b = g\phi_m(x,t)\bar{\varepsilon}^2(s(x,t))h_t^2(s(x,t)) + g\bar{\varepsilon}^2(s(x,t)) + \frac{3}{2}\phi_m^2(x,t)$ and multiply (42) by $e^{\lambda t}$

$$\dot{V}(t)e^{\lambda t} \le -\lambda V(t)e^{\lambda t} + be^{\lambda t} \tag{43}$$

Then, by integrating both sides of (43), we have

$$V(t) \le V(0)e^{-\lambda t} + \frac{b}{\lambda}(1 - e^{-\lambda t}) \tag{44}$$

The following inequality is then obtained

$$\frac{1}{2}\|w(x,t)\|^2 \le V_2(t) \le V(t) \tag{45}$$

Considering (44), we have

$$\lim_{t\to\infty} \|w(x,t)\| \le \sqrt{\frac{2b}{\lambda}}, \tag{46}$$

Thus, the closed-loop MAS is uniformly ultimately bounded by choosing appropriate system parameters.

We discretize the PDE model (8) using the finite difference method, allowing us to implement the proposed control method when the number of agents is limited. Different finite-difference methods result in distinct communication network topologies. In this study, we opt for the three-point central difference method, which gives rise to a chain-like topology (illustrated in Fig. 2). The defined communication topology graph is undirected and comprises n nodes, with each node representing an agent positioned at that node. Given that the desired curve is closed in C^2, it is reasonable to assume that the chain-like communication topology is also closed.

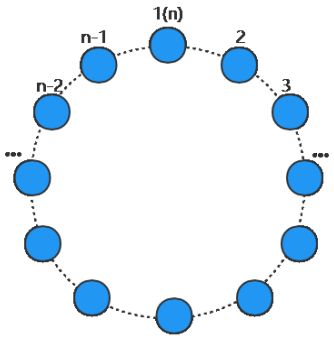

Fig. 2. Communication relationship between agents.

VI. Simulations

In this section, numerical simulation examples are employed to validate the theoretical findings. Utilizing the estimated state of the agent acquired through the observer (9) and integrating it with the RBF neural network, a controller (27) with network adaptation law (28) is derived to guide the MAS from its initial position to the target position. The detailed procedure is outlined in Procedure 1. The MATLAB simulation program is found on the finite difference method, and The number of simulated agents n is 40. Each agent's initial position $z(x,0)$ is evenly distributed along the coordinates $\left(0.5 * \sin\left(i\frac{2\pi}{n}\right), 0.5 * \cos\left(i\frac{2\pi}{n}\right), 0\right)$, where $i = 1, \ldots, n$. As for the C^2 curve target, we provide the target position $\gamma(x)$ evenly distributed across $(\sin(\alpha), \cos\alpha, \sin(\alpha)\cos(\alpha) + 5)$.

In the MAS deployment figure, the red and blue dashed lines, respectively, represent the target formation and the initial positions of the MAS agents. Each solid gray line represents the trajectory of an agent as it moves in 3D space. In the tracking error and error system figures, each solid line corresponds to the tracking error and estimation error of the respective agent.

We begin with the scenario where there is no system uncertainty. The adjustable system parameters are configured as follows: $a = 6$, $k = 1.8$, and $P = 2.4$. As depicted in Fig.3, the agents successfully reach the desired spatial location. This demonstrates that the proposed control method facilitates the deployment of the networked MAS onto the desired C^2 curve. Figs.4-6 display the tracking errors of the agents along the x, y, and z axes. It is evident that these errors ultimately converge to zero in a short time. Figs. 7-9 depict the discrepancies between the actual state of the agent and the estimated state of the observer, showcasing the observer's good performance.

Next, we provide an example for the scenario involving system uncertainty. The adjustable system parameters are

Procedure 1 The Flowchart of Observer-Based Feedback Control Scheme With RBF Neural Network for Multi-Agent Systems

Steps	Descriptions
Step 1: Build system model	Given in (8);
Step 2: Consider the observer	$\hat{w}_t(x,t) = a\hat{w}_{xx}(x,t) + u(x,t) + P\tilde{w}(\pi,t);$
Step 3: Introduce the RBF neural network	$\|f_i(s_i(x,t))\| = W_i^{*T}h_i(s_i(x,t)) + \varepsilon_i(s_i(x,t));$
Step 4: Design the observer-based control law	$u_i(x,t) = -\frac{g\hat{\phi}_i h^T(\hat{s}_i(x,t))h(\hat{s}_i(x,t))}{2\pi\hat{w}_i(x,t)} - k\hat{w}_i(x,t) - P\tilde{w}_i(\pi,t);$
Step 5: Update estimated parameters	$\dot{\hat{\phi}}_i = \frac{g\beta h^T(\hat{s}_i(x,t))h(\hat{s}_i(x,t))}{2\pi} - \beta\hat{\phi}_i;$
Step 6: Numerical Simulations;	

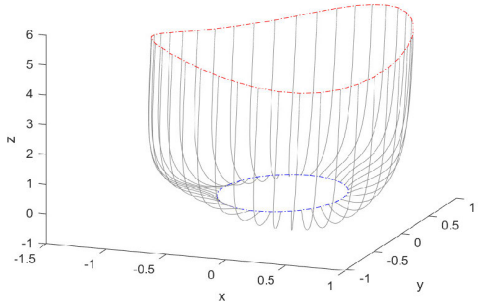

Fig. 3. Real-time deployment trajectory of the multi-agent system.

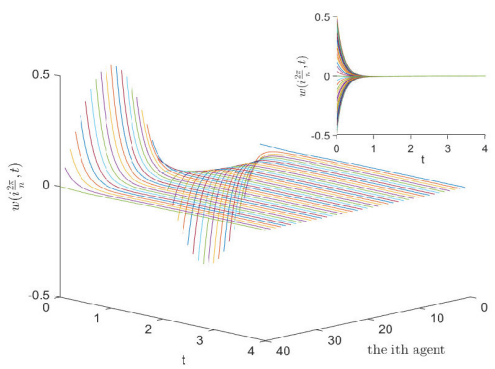

Fig. 4. The tracking error on x-axes.

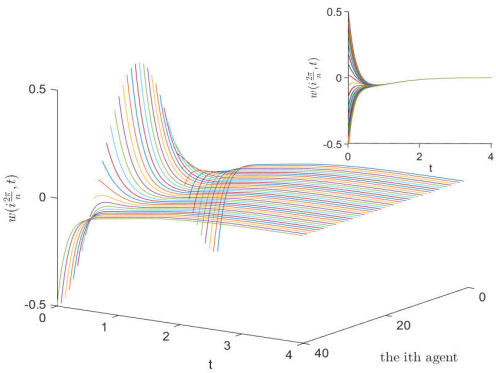

Fig. 5. The tracking error on y-axes.

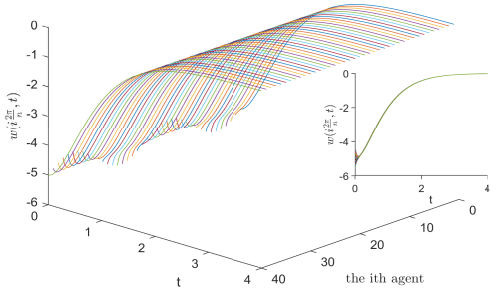

Fig. 6. The tracking error on z-axes.

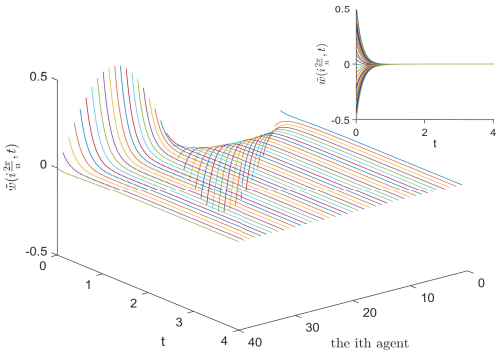

Fig. 7. The state of the error system (10) on x-axes.

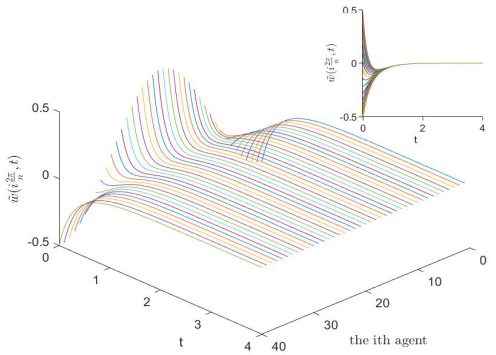

Fig. 8. The state of the error system (10) on y-axes.

configured as follows: $a = 6.4$, $k = 5$, $P = 2.6$, and $\beta = 1$. The system uncertainty of the MAS is defined as $f(s(x,t)) = w(x,t)w_t(x,t)$. The matrices μ_i and η_i are set as $\mu_i = \begin{bmatrix}-1 & -0.5 & 0 & 0.5 & 1 & -6 & -3 & 0 & 3 & 6\end{bmatrix}$ and $\eta_i = 1$. Fig. 10 illustrates the performance of MAS deployment with system uncertainty, demonstrating that the agents successfully achieve

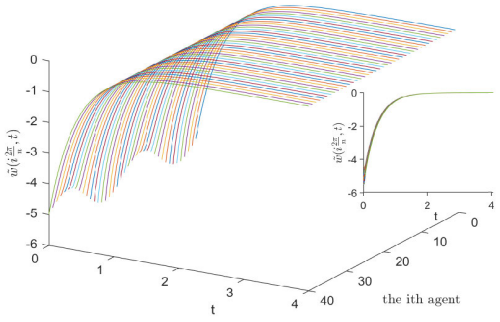

Fig. 9. The state of the error system (10) on z-axes.

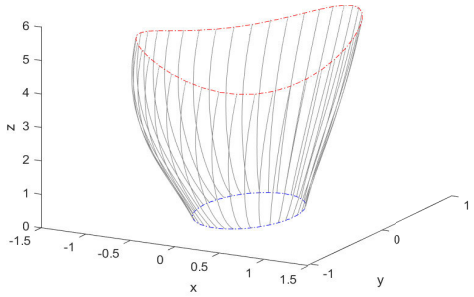

Fig. 10. Real-time deployment trajectory of the multi-agent system after using RBF neural networks to deal with the uncertainty of the system.

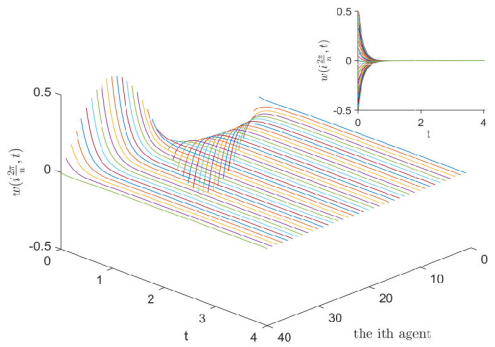

Fig. 11. The tracking error of the multi-agent system with RBF neural networks on x-axes.

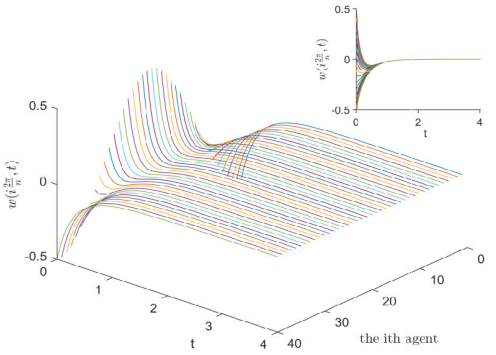

Fig. 12. The tracking error of the multi-agent system with RBF neural networks on y-axes.

the desired control objective while dealing with the existing system uncertainty. Figs.11-13 depict the tracking errors in each coordinate. After a brief tuning period, the tracking errors

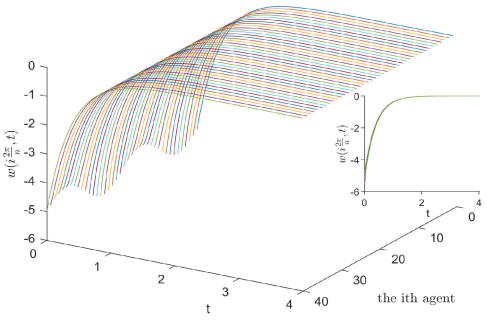

Fig. 13. The tracking error of the multi-agent system with RBF neural networks on z-axes.

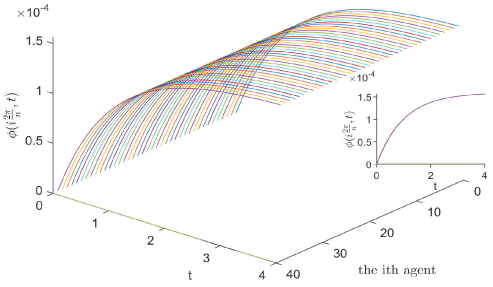

Fig. 14. The norm of the weight of the neural network on x-axes.

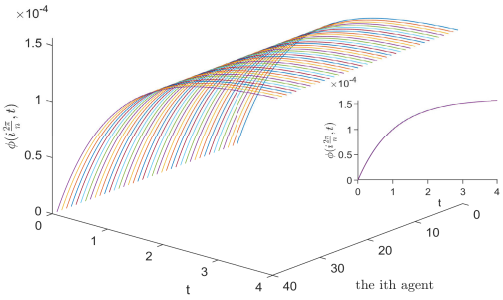

Fig. 15. The norm of the weight of the neural network on y-axes.

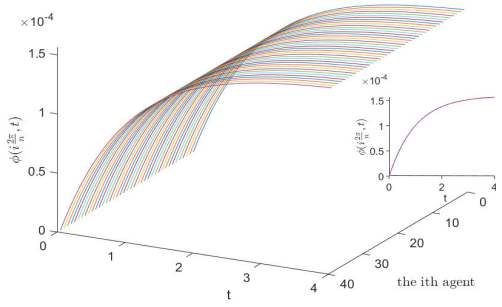

Fig. 16. The norm of the weight of the neural network on z-axes.

of the agents converge to very small values. The evolution of the neural network weight matrix norm parameter is illustrated in Figs. 14-16. The results indicate that in scenarios where system uncertainty exists, the incorporation of RBF neural networks enables the tracking error to converge to zero within 2 seconds, matching the convergence speed observed in situations without system uncertainty. This highlights the significant advantage of the adaptive control method proposed

in this paper, which utilizes neural networks to effectively address system uncertainty.

VII. Conclusion

This study was primarily focused on a deployment methodology for MAS in 3D space. A non-collocated observer was introduced to address the issue of incomplete state information for the agents, with only a designated agent having access to its own location information. The uncertainty present in the MAS was approximated using an RBF neural network. Through Lyapunov's theory, it was established that the closed-loop MAS was uniformly ultimately bounded. It was demonstrated that the MAS could converge to any closed C^2 curve by appropriately selecting system parameters. Future research directions include the investigation of fault estimation and fault-tolerant control for nonlinear MASs.

References

[1] Y. Zhao, H. Liang, G. Zong, and H. Wang, "Event-based distributed finite-horizon $\mathcal{H}_\infty$ consensus control for constrained nonlinear multiagent systems," *IEEE Syst. J.*, vol. 17, no. 4, pp. 5369–5380, Dec. 2023.

[2] F. Cheng, B. Niu, N. Xu, and X. Zhao, "Resilient distributed secure consensus control for uncertain networked agent systems under hybrid DoS attacks," *Commun. Nonlinear Sci. Numer. Simul.*, vol. 129, Feb. 2024, Art. no. 107689.

[3] L. Tian, Y. Hua, X. Dong, J. Lü, and Z. Ren, "Distributed time-varying group formation tracking for multiagent systems with switching interaction topologies via adaptive control protocols," *IEEE Trans. Ind. Informat.*, vol. 18, no. 12, pp. 8422–8433, Dec. 2022.

[4] M. Brittain and P. Wei, "Scalable autonomous separation assurance with heterogeneous multi-agent reinforcement learning," *IEEE Trans. Autom. Sci. Eng.*, vol. 19, no. 4, pp. 2837–2848, Oct. 2022.

[5] F. Cheng, H. Liang, H. Wang, G. Zong, and N. Xu, "Adaptive neural self-triggered bipartite fault-tolerant control for nonlinear MASs with dead-zone constraints," *IEEE Trans. Autom. Sci. Eng.*, vol. 20, no. 3, pp. 1–12, Jul. 2022.

[6] H. Zhong, J. Liang, Y. Chen, H. Zhang, J. Mao, and Y. Wang, "Prototype, modeling, and control of aerial robots with physical interaction: A review," *IEEE Trans. Autom. Sci. Eng.*, early access, May 6, 2024, doi: 10.1109/TASE.2024.3395658.

[7] K.-K. Oh, M.-C. Park, and H.-S. Ahn, "A survey of multi-agent formation control," *Automatica*, vol. 53, pp. 424–440, Mar. 2015.

[8] K.-K. Oh and H.-S. Ahn, "Formation control of mobile agents based on distributed position estimation," *IEEE Trans. Autom. Control*, vol. 58, no. 3, pp. 737–742, Mar. 2013.

[9] S.-M. Kang and H.-S. Ahn, "Design and realization of distributed adaptive formation control law for multi-agent systems with moving leader," *IEEE Trans. Ind. Electron.*, vol. 63, no. 2, pp. 1268–1279, Feb. 2016.

[10] Y. Hua, X. Dong, L. Han, Q. Li, and Z. Ren, "Finite-time time-varying formation tracking for high-order multiagent systems with mismatched disturbances," *IEEE Trans. Syst., Man, Cybern., Syst.*, vol. 50, no. 10, pp. 3795–3803, Oct. 2020.

[11] G. Freudenthaler and T. Meurer, "PDE-based multi-agent formation control using flatness and backstepping: Analysis, design and robot experiments," *Automatica*, vol. 115, May 2020, Art. no. 108897.

[12] J. Qi, S. Wang, J.-A. Fang, and M. Diagne, "Control of multi-agent systems with input delay via PDE-based method," *Automatica*, vol. 106, pp. 91–100, Aug. 2019.

[13] P. Frihauf and M. Krstic, "Leader-enabled deployment onto planar curves: A PDE-based approach," *IEEE Trans. Autom. Control*, vol. 56, no. 8, pp. 1791–1806, Aug. 2011.

[14] J. Qi and M. Krstic, "Compensation of spatially varying input delay in distributed control of reaction-diffusion PDEs," *IEEE Trans. Autom. Control*, vol. 66, no. 9, pp. 4069–4083, Sep. 2021.

[15] Q. Qiu and H. Su, "Distributed adaptive consensus of parabolic PDE agents on switching graphs with relative output information," *IEEE Trans. Ind. Informat.*, vol. 18, no. 1, pp. 297–304, Jan. 2022.

[16] G. Ferrari-Trecate, A. Buffa, and M. Gati, "Analysis of coordination in multi-agent systems through partial difference equations," *IEEE Trans. Autom. Control*, vol. 51, no. 6, pp. 1058–1063, Jun. 2006.

[17] J. Man, Y. Sheng, C. Chen, and Z. Zeng, "PDE-based finite-time deployment of heterogeneous multi-agent systems subject to multiple asynchronous semi-Markov chains," *IEEE Trans. Circuits Syst. I, Reg. Papers*, vol. 71, no. 2, pp. 885–897, Feb. 2024.

[18] G. Freudenthaler and T. Meurer, "PDE-based tracking control for multi-agent deployment," *IFAC-PapersOnLine*, vol. 49, no. 18, pp. 582–587, 2016.

[19] J. Liang, H. Zhong, Y. Wang, Y. Chen, J. Zeng, and J. Mao, "Adaptive force tracking impedance control for aerial interaction in uncertain contact environment using barrier function," *IEEE Trans. Autom. Sci. Eng.*, early access, Aug. 9, 2024, doi: 10.1109/TASE.2023.3301023.

[20] Y. Li, S. Dong, K. Li, and S. Tong, "Fuzzy adaptive fault tolerant time-varying formation control for nonholonomic multirobot systems with range constraints," *IEEE Trans. Intell. Veh.*, vol. 8, no. 6, pp. 3668–3679, Jun. 2023.

[21] Y. Zhang, C. Edwards, M. Belmont, and G. Li, "Robust model predictive control for constrained linear system based on a sliding mode disturbance observer," *Automatica*, vol. 154, Aug. 2023, Art. no. 111101.

[22] L. Ma, F. Zhu, and X. Zhao, "Human-in-the-loop consensus control for multiagent systems with external disturbances," *IEEE Trans. Neural Netw. Learn. Syst.*, vol. 35, no. 8, pp. 11024–11034, Aug. 2023.

[23] J. Chen, Y. Wu, and H. Qiao, "Memory, attention, and muscle synergies based reinforcement and transfer learning for musculoskeletal robots under imperfect observation," *IEEE/ASME Trans. Mechatronics*, early access, May 24, 2024, doi: 10.1109/TMECH.2024.3401045.

[24] F. Wang, C. Zhang, Y. Yang, and N. Li, "Observer-based consensus of fractional order parabolic PDEs agents on directed networks via boundary communication," *Chaos, Solitons Fractals*, vol. 170, May 2023, Art. no. 113332.

[25] B. Rathnayake, M. Diagne, N. Espitia, and I. Karafyllis, "Observer-based event-triggered boundary control of a class of reaction–diffusion PDEs," *IEEE Trans. Autom. Control*, vol. 67, no. 6, pp. 2905–2917, Jun. 2022.

[26] A. U. Levin and K. S. Narendra, "Control of nonlinear dynamical systems using neural networks. II. Observability, identification, and control," *IEEE Trans. Neural Netw.*, vol. 7, no. 1, pp. 30–42, Jan. 1996.

[27] S. Seshagiri and H. K. Khalil, "Output feedback control of nonlinear systems using RBF neural networks," *IEEE Trans. Neural Netw.*, vol. 11, no. 1, pp. 69–79, Jan. 2000.

[28] S. Wang and D. L. Yu, "Adaptive RBF network for parameter estimation and stable air–fuel ratio control," *Neural Netw.*, vol. 21, no. 1, pp. 102–112, Jan. 2008.

[29] Z. Chen, F. Huang, W. Sun, J. Gu, and B. Yao, "RBF-neural-network-based adaptive robust control for nonlinear bilateral teleoperation manipulators with uncertainty and time delay," *IEEE/ASME Trans. Mechatronics*, vol. 25, no. 2, pp. 906–918, Apr. 2020.

[30] B. Yan, J. Ni, Y. Zhong, D. Yu, and Z. Wang, "Collision-free formation control for heterogeneous multiagent systems under DoS attacks," *IEEE Trans. Cybern.*, early access, Jul. 25, 2024, doi: 10.1109/TCYB.2024.3418973.

[31] Z. Kan, J. M. Shea, and W. E. Dixon, "Leader–follower containment control over directed random graphs," *Automatica*, vol. 66, pp. 56–62, Apr. 2016.

[32] Y. Li, C. Hua, S. Wu, and X. Guan, "Output feedback distributed containment control for high-order nonlinear multiagent systems," *IEEE Trans. Cybern.*, vol. 47, no. 8, pp. 2032–2043, Aug. 2017.

[33] H. Li, J. Luo, H. Ma, and Q. Zhou, "Observer-based event-triggered iterative learning consensus for locally Lipschitz nonlinear mass," *IEEE Trans. Cogn. Develop. Syst.*, vol. 16, no. 1, pp. 46–56, Feb. 2024.

[34] D. J. H. Garling, *Inequalities: A Journey Into Linear Analysis*. Cambridge, U.K.: Cambridge Univ. Press, 2007.

[35] Z. Han, Z. Liu, L. Kong, L. Ding, J.-W. Wang, and W. He, "Adaptive fuzzy control for a hybrid spacecraft system with spatial motion and communication constraints," *IEEE Trans. Fuzzy Syst.*, vol. 30, no. 8, pp. 3247–3256, Aug. 2022.

[36] Y. Wu, W. Niu, L. Kong, X. Yu, and W. He, "Fixed-time neural network control of a robotic manipulator with input deadzone," *ISA Trans.*, vol. 135, pp. 449–461, Apr. 2023.

[37] L. Kong, W. He, Y. Dong, L. Cheng, C. Yang, and Z. Li, "Asymmetric bounded neural control for an uncertain robot by state feedback and output feedback," *IEEE Trans. Syst., Man, Cybern., Syst.*, vol. 51, no. 3, pp. 1735–1746, Mar. 2021.

[38] J.-L. Wang, H.-N. Wu, and L. Guo, "Novel adaptive strategies for synchronization of linearly coupled neural networks with reaction-diffusion terms," *IEEE Trans. Neural Netw. Learn. Syst.*, vol. 25, no. 2, pp. 429–440, Feb. 2014.

[39] A. Mostaani, T. X. Vu, S. Chatzinotas, and B. Ottersten, "Task-effective compression of observations for the centralized control of a multiagent system over bit-budgeted channels," *IEEE Internet Things J.*, vol. 11, no. 4, pp. 6131–6143, Feb. 2024.

[40] J. Chen and H. Qiao, "Motor-cortex-like recurrent neural network and multitask learning for the control of musculoskeletal systems," *IEEE Trans. Cogn. Develop. Syst.*, vol. 14, no. 2, pp. 424–436, Jun. 2022.

[41] T. Zhang, S. S. Ge, and C. C. Hang, "Adaptive neural network control for strict-feedback nonlinear systems using backstepping design," *Automatica*, vol. 36, no. 12, pp. 1835–1846, 2000.

Zhijie Liu (Member, IEEE) received the B.Sc. degree from China University of Mining and Technology Beijing, Beijing, China, in 2014, and the Ph.D. degree from Beihang University, Beijing, in 2019. In 2017, he was a Research Assistant with the Department of Electrical Engineering, University of Notre Dame, for 12 months. He is currently a Full Professor with the School of Intelligence Science and Technology, University of Science and Technology Beijing, Beijing. His research interests include adaptive control, modeling and vibration control for flexible structures, and distributed parameter systems.

Jianhui Zhang received the B.Eng. degree from the Qilu University of Technology, Jinan, China, in 2015, and the M.Eng. degree from Shandong University of Science and Technology, Qingdao, China, in 2020. He is currently pursuing the Ph.D. degree in control science and engineering with the School of Intelligence Science and Technology, University of Science and Technology Beijing, Beijing, China. His research interests include flapping wing robots, multi-agent, and neural network control.

Huiyang Song received the B.Eng. degree from Northeastern University, Shenyang, China, in 2020, and the M.Eng. degree from the University of Science and Technology Beijing, Beijing, China, in 2023. His research interests include multi-agent and neural network control.

Yan Yang received the B.Eng. degree from Xi'an University of Science and Technology, Xi'an, China, in 2011, and the M.Eng. and Ph.D. degrees from Xidian University, Xi'an, in 2019. She is currently a Full Lecturer with the School of Intelligence Science and Technology, University of Science and Technology Beijing, Beijing, China. Her research interests include discrete event systems, supervisory control and applications, multi-agent, system security, and concealment analysis and control.

Zhijia Zhao (Member, IEEE) received the B.Eng. degree in automatic control from the North China University of Water Resources and Electric Power, Zhengzhou, China, in 2010, and the M.Eng. and Ph.D. degrees in automatic control from the South China University of Technology, Guangzhou, China, in 2013 and 2017, respectively. He is currently an Associate Professor with the School of Mechanical and Electrical Engineering, Guangzhou University. His research interests include adaptive and learning control, flexible mechanical systems, and robotics.

Keum-Shik Hong (Fellow, IEEE) received the B.S. degree in mechanical design from Seoul National University in 1979, the M.S. degree in mechanical engineering from Columbia University, New York, in 1987, and the M.S. degree in applied mathematics and the Ph.D. degree in mechanical engineering from the University of Illinois at Urbana–Champaign, Champaign, IL, USA, in 1991. He joined the School of Mechanical Engineering, Pusan National University, in 1993. His research interests include brain–computer interface, nonlinear systems theory, adaptive control, and distributed parameter systems. He is a fellow of the Korean Academy of Science and Technology, an ICROS Fellow, and a member of the National Academy of Engineering of Korea. He has received many awards, including the Best Paper Award from the KFSTS of Korea in 1999 and the Presidential Award of Korea in 2007. He served as an Associate Editor for *Automatica* from 2000 to 2006, the Editor-in-Chief for the *Journal of Mechanical Science and Technology* from 2008 to 2011, and the Editor-in-Chief for the *International Journal of Control, Automation, and Systems*. He was the President of the Institute of Control, Robotics, and Systems (ICROS), South Korea, and the Asian Control Association.